ChemComm

Validation of a Post-Radiolabeling Bioconjugation Strategy for Radioactive Rare Earth Complexes with Minimal Structural Footprint

Journal:	*ChemComm*
Manuscript ID	CC-COM-11-2022-006128.R1
Article Type:	Communication

COMMUNICATION

Validation of a Post-Radiolabeling Bioconjugation Strategy for Radioactive Rare Earth Complexes with Minimal Structural Footprint

Received 00th January 20xx,
Accepted 00th January 20xx

DOI: 10.1039/x0xx00000x

Raphael Lengacher,[a] Alexia G. Cosby,[a] Dariusz Śmiłowicz,[a] Eszter Boros* [a]

[a]Department of Chemistry, Stony Brook University, 100 Nicolls Road, Stony Brook, NY 11794, USA.

The nine-coordinate aza-macrocycle DO3Apic-NO_2 and its kinetically inert rare earth complexes [M(DO3A-pic-NO_2)]$^-$ (M= La, Tb, Eu, Lu, Y) can be readily bioconjugated to surface accessible thioles on peptides and proteins with a minimal structural footprint. All complexes express thioconjugation rate constants in the same order of magnitude (k = 0.3 h^{-1}) with the exception of Sc (k = 0.89 h^{-1}). Coupling to peptides and biologics with accessible cysteines also enables post-radiochelation bioconjugation at room temperature to afford injection-ready radiopharmaceuticals as demonstrated by formation of [^{177}Lu][Lu(DO3Apic-NO_2)]$^-$ and [^{86}Y][Y(DO3Apic-NO_2)]$^-$, followed by post-labeling conjugation to a cysteine-functionalized peptide targeting the prostate specific membrane antigen. The ^{86}Y-labeled construct efficiently localizes in target tumors with no significant off-target accumulation as evidenced by positron emission tomography, biodistribution studies and metabolite analysis.

Emerging radioactive rare earth isotopes such as ^{177}Lu (β^-(max) = 501 keV, $t_{1/2}$ = 6.64 d), ^{86}Y (β^+(max) = 4.2 MeV, $t_{1/2}$ = 14.7 h), and $^{44/47}$Sc (^{44}Sc: β^+(max) = 2.6 MeV, $t_{1/2}$ = 3.97 h; ^{47}Sc: β^-(max) = 600 keV, $t_{1/2}$ = 3.35 d) offer promising avenues for the development of diagnostic and therapeutic radiopharmaceuticals.[1] Additionally, their stable isotopologues are well suited for the introduction of spin-tags (Gd)[2-4] and luminescence markers (Tb, Eu, Sm).[5] However, on their own, they possess no ability to localize in specific tissues of interest and must therefore be appended to targeting vectors that enable accumulation in sites of interest. Biological targeting vectors such as peptides, monoclonal antibodies, antibody fragments, or affibodies are of specific interest due to their high target specificity; a plethora of bioconjugated radionuclides have been reported and several have been approved for routine clinical use.[6]

However, the incorporation of these isotopes into thermally sensitive biomolecules can be challenging. The most common approach is the incorporation of a chelator in a first step, followed by coordination to the desired radiometal in a second, penultimate step.[7-10] This works well for chelator-radionuclide pairs that form readily and rapidly at room temperature. Such systems frequently exhibit poor long-term kinetic inertness which can lead to loss of the radiometal in vivo prior to deposition in the target tissue. Alternatively, more kinetically inert systems can be employed but because these require temperatures above 40°C for efficient radiolabeling, compatibility with the thermally sensitive nature of biologics is diminished (Figure S2).[11, 12] A possible solution is to employ post-labeling bioconjugation strategies, which involves pre-formation of a thermodynamically stable and kinetically inert radiochemical complex at elevated temperature, followed by its conjugation to the targeting vector under comparatively mild conditions. This requires (1) bioconjugation reactions with fast kinetics, to minimize radioactive decay during the radiosynthetic process and (2) the functionalization of the biomolecule with the corresponding bioconjugation partner prior to the actual bioconjugation reaction. While this approach has been successfully validated using a metal-chelate functionalized

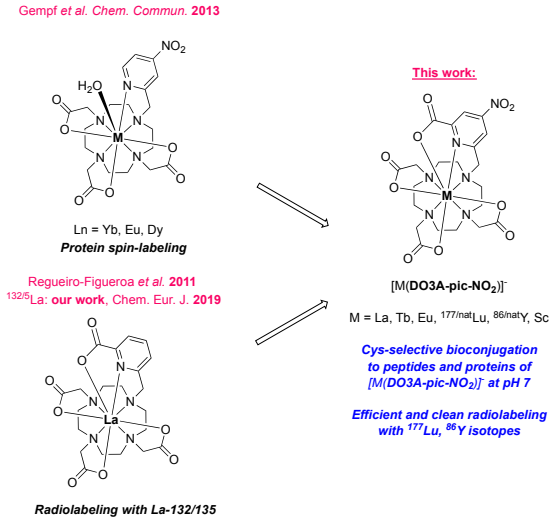

Figure 1: Summary of the work presented in this article in context of prior art. [M(**DO3A-pic-NO_2**)]$^-$ can be readily radiolabeled and subsequently conjugated to cysteine residues of peptides/proteins at pH 7 and 37 °C, producing ready-to-inject radiopharmaceuticals.

tetrazine and trans-cyclooctene appended antibodies, the limited long-term stability and hydrophobicity of tetrazines can pose challenges.[13]

Here, we address these shortcomings by bioconjugation of kinetically inert rare earth complexes that do not require prior functionalization of the targeting vector and retain a minimal structural footprint and high complex hydrophilicity. To this end, we explored the selective thioreactivity of nitropyridine and nitropicolinate lanthanide complexes inspired by the 8-coordinate **DO3A-pyr-NO$_2$** system established by Butler and Parker.[14-17] We proposed that this reaction was well suited for a post-labeling conjugation strategy to append kinetically inert, radioactive, rare earth complexes to reactive, native thiols present on peptides and biologics. We validated this hypothesis by synthesis and characterization of select rare earth complexes of the 9-coordinate chelator **DO3A-pic-NO$_2$** and profile their reactivity for thioconjugation, radiochemical labeling efficiency and subsequent, direct in vivo administration for targeted PET imaging.

The chemical synthesis of **DO3A-pic-NO$_2$** was adapted from literature procedures for nitropicolinate-functionalized chelators.[4, 15, 18] Chelation of **DO3A-pic-NO$_2$** was conducted using M^{3+} salt (M = La, Eu, Tb, Lu, Y, Sc) to produce [M(**DO3A-pic-NO$_2$**)]$^-$.

Next, we probed the kinetics of thioether formation using thiol ethyl thioglycolate (HS-R$_1$, **HSEtCOOEt**) at 1:1 complex to thiol ratio (Figure 2A). Thioether formation was monitored a characteristic shift in the UV absorbance from 300 nm to 280 nm (Figure S5).[15] We observed no significant difference for the conjugation rate among different rare earth complexes probed, with the exception of [Sc(**DO3A-pic-NO$_2$**)]$^-$ (k = 0.89 h^{-1}, $t_{1/2}$ = 1.1 h), all k-values fall into the same range and order of magnitude of 0.3 h^{-1} ($t_{1/2}$ = 3.3 h) (Figure 2B, Table S1). Characterization of the photophysical properties of [Tb(**DO3A-pic-NO$_2$**)]$^-$ and [Tb(**DO3A-pic-SEtCOOEt**)]$^-$ was also conducted (Table S2) to affirm no inner sphere hydration of the corresponding coordination complexes.

To probe the scope of reactivity, we also tested conjugation to cysteine thioles using a cysteine-functionalized tetra-peptide HS-Cys-PSMA (HS-R$_2$) and bovine serum albumin (HS-R$_3$, BSA), which possesses a single, reactive cysteine residue, Cys34. Both biomolecules were conjugated successfully as indicated by chromatographic and mass spectrometric analysis (Figures S4, S13-S15).

Next, we tested **DO3A-pic-NO$_2$** for radiochemical applications with ^{177}Lu and ^{86}Y using a post-radiolabeling conjugation approach (Figure 3A). Quantitative labeling was achieved for 0.25 - 0.5 nmol of **DO3A-pic-NO$_2$** (25 mM NH_4OAc buffer at pH = 5.5) in 15 min at 80°C (Figure 3B), producing an apparent molar activity of 0.248 mCi/nmol for ^{177}Lu and 0.022 mCi/nmol for ^{86}Y (Figure S8). Complex identity was confirmed by coinjection with the isolated ^{nat}Lu/ ^{nat}Y species (Figure S9).

Freshly prepared solutions of [^{177}Lu][Lu(**DO3A-pic-NO$_2$**)]$^-$ and [^{86}Y][Y(**DO3A-pic-NO$_2$**)]$^-$ were cooled to room temperature and incubated with 6-30 equivalents of cysteine functionalized PSMA targeting peptide H**S-Cys-PSMA** (HS-R$_2$, see Supporting Information). The reaction was conducted at pH 7.5 and 37°C in presence of tris(2-carboxyethyl)phosphine (TCEP,1.25 eq.) to prevent the formation of disulfide bonds (Figure 3A). The reaction achieved 69% conversion after 4 h (Figures S12, S14) for [^{177}Lu][Lu(**DO3A-pic-S-Cys-PSMA**)]$^-$ and 54% conversion after 10 h (Figure 3B) for [^{86}Y][Y(**DO3A-pic-S-Cys-PSMA**)]$^-$. To demonstrate the feasibility of a direct bioconjugation to injection approach, [^{86}Y][Y(**DO3A-pic-S-Cys-PSMA**)]$^-$ containing unreacted [^{86}Y][Y(**DO3A-pic-NO$_2$**)]$^-$ was administered without further purification to mice bearing bilateral xenografts with or without PSMA expression. PET imaging at 90 min post injection (Figure 3C) and biodistribution analysis at 2 h (Figure 3D) showed rapid, renal clearance, statistically significant target tumor uptake (6.1% ID/g, Figure 3D, pink bars) and no notable off-target accumulation indicative of radiometal dissociation. Analysis of urine metabolites showed presence of [^{86}Y][Y(**DO3A-pic-S-Cys-PSMA**)]$^-$ (Figure 3B, bottom trace). A corresponding control biodistribution experiment with [^{86}Y][Y(**DO3A-pic-NO$_2$**)]$^-$ showed low accumulation in all analyzed organs and no target-specific accumulation in the tumor (0.2% ID/g, Figure 3D, grey bars), demonstrating that the post-labeling conjugation approach produced a functional, targeted imaging agent with high kinetic inertness and efficacy. Of note, all ^{177}Lu

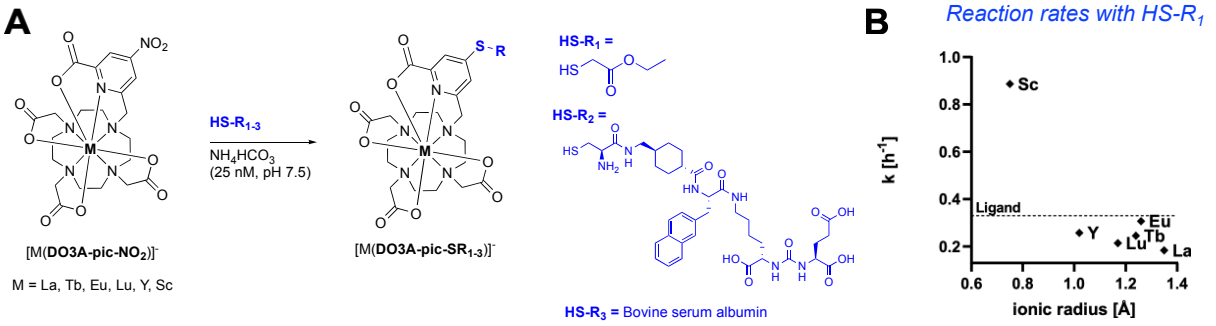

Figure 2. A: Reaction scheme of the thioconjugation between [M(**DO3A-pic-NO$_2$**)]$^-$ and **HS-R$_{1-3}$**, resulting in the formation of [M(**DO3A-pic-SR$_{1-3}$**)]$^-$ complexes characterized in this work at r.t. in ammonium bicarbonate buffer at pH 7.5. **B:** Plot of k-values [h^{-1}] versus ionic radii [Å] of the employed M^{3+} ions demonstrating that ligand and corresponding complexes exhibit comparable reaction rates except for M=Sc.

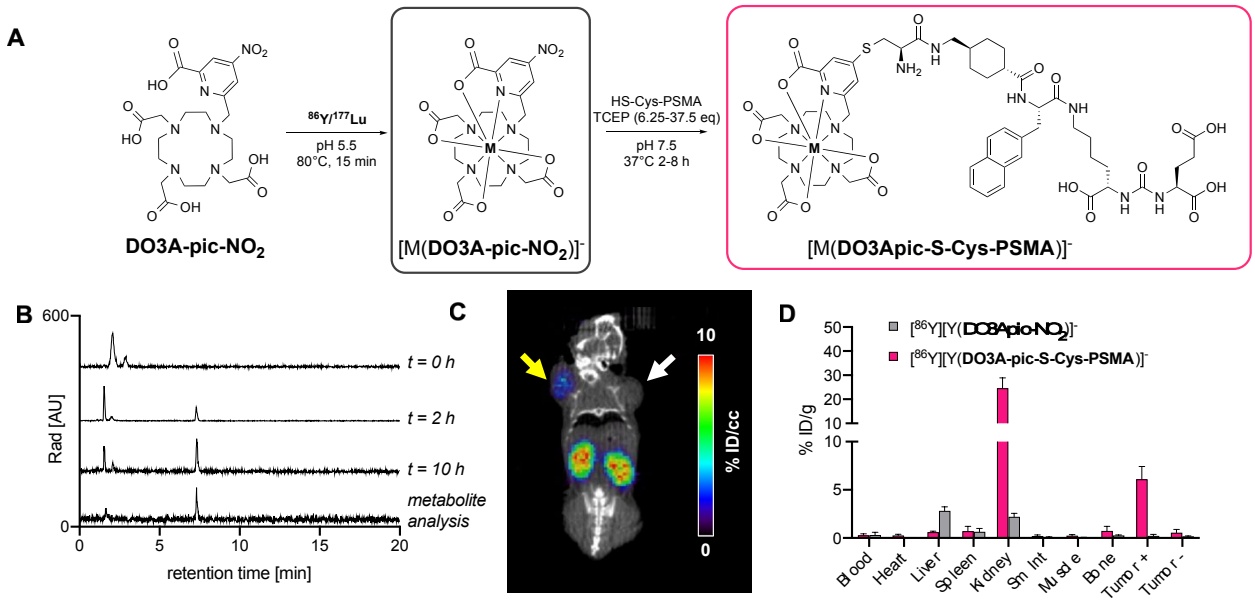

Figure 3: A: Reaction scheme for the radiolabeling of **DO3A-pic-NO$_2$** and subsequent thioconjugation. **B:** RadioHPLC monitoring of the reaction progress for the formation of [^{86}Y][Y(**DO3A-pic-S-Cys-PSMA**)]$^-$ at = 2 and 10 hours – urine metabolite analysis indicates that the complex is stable in vivo. **C:** Coronal PET image of [^{86}Y][Y(**DO3A-pic-S-Cys-PSMA**)]$^-$ 90 minutes post-injection shows target tumor uptake (yellow arrow) while PSMA-non-expressing tumor shows no uptake. **D**: Selective tumor uptake of [^{86}Y][Y(**DO3A-pic-S-Cys-PSMA**)]$^-$ is further affirmed by 2 h p.i. biodistribution analysis (pink) while [^{86}Y][Y(**DO3A-pic-NO$_2$**)]$^-$shows rapid clearance and no accumulation in off-target organs (grey bars).

and ^{86}Y labeled complexes retained high solubility in aqueous media and did not require formulation with organic co-solvents.

Conclusively, the [M(**DO3A-NO$_2$**)]$^-$ platform allows for the post-radiolabeling bioconjugation to cysteine residues at 37°C, enabling efficient labeling of targeting vectors with a kinetically inert radiochemical ^{86}Y/^{177}Lu-complex for targeted in vivo imaging and therapy applications.

All authors have contributed to the manuscript. There are no conflicts to declare. The authors acknowledge funding sources, specifically the NIH for a NIBIB R21 Trailblazer award (R21EB030071-01A1) and the National Science Foundation for an NSF CAREER (CHE 1942434). Electronic Supplementary Information (ESI) available: chemical synthesis, characterization, and relevant experimental details for radiolabeling and animal work are provided.

References

1. T. I. Kostelnik and C. Orvig, *Chem. Rev.*, 2019, **119**, 902-956.
2. L. M. Mitsumori, P. Bhargava, M. Essig and J. H. Maki, *Top. Magn. Reson. Imaging*, 2014, **23**, 51-69.
3. E. C. Giese, *Clin Med Rep*, 2018, **2**, 1-2.
4. M. Regueiro-Figueroa, B. Bensenane, E. Ruscsák, D. Esteban-Gómez, L. J. Charbonnière, G. Tircsó, I. Tóth, A. d. Blas, T. Rodríguez-Blas and C. Platas-Iglesias, *Inorg. Chem.*, 2011, **50**, 4125-4141.
5. J. A. Adewuyi, N. D. Schley and G. Ung, *Inorg. Chem. Front.*, 2022, **9**, 1474-1480.
6. D. J. Vugts and G. A. M. S. van Dongen, in *Radiopharmaceutical Chemistry*, eds. J. S. Lewis, A. D. Windhorst and B. M. Zeglis, Springer International Publishing, Cham, 2019, DOI: 10.1007/978-3-319-98947-1_9, pp. 163-179.
7. R. Rossin, P. Renart Verkerk, S. M. van den Bosch, R. C. M. Vulders, I. Verel, J. Lub and M. S. Robillard, *Angew. Chem. Int. Ed.*, 2010, **49**, 3375-3378.
8. P. Adumeau, K. E. Carnazza, C. Brand, S. D. Carlin, T. Reiner, B. J. Agnew, J. S. Lewis and B. M. Zeglis, *Theranostics*, 2016, **6**, 2267-2277.
9. J.-P. Meyer, J. L. Houghton, P. Kozlowski, D. Abdel-Atti, T. Reiner, N. V. K. Pillarsetty, W. W. Scholz, B. M. Zeglis and J. S. Lewis, *Bioconjug. Chem.*, 2016, **27**, 298-301.
10. S. M. J. van Duijnhoven, R. Rossin, S. M. van den Bosch, M. P. Wheatcroft, P. J. Hudson and M. S. Robillard, *J. Nucl. Med.*, 2015, **56**, 1422.
11. R. Chakravarty, S. Chakraborty, H. D. Sarma, K. V. V. Nair, A. Rajeswari and A. Dash, *J. Labelled Compd. Radiopharm.*, 2016, **59**, 354-363.
12. A. Majkowska-Pilip and A. Bilewicz, *J. Inorg. Biochem.*, 2011, **105**, 313-320.
13. Z. Li, H. Cai, M. Hassink, M. L. Blackman, R. C. D. Brown, P. S. Conti and J. M. Fox, *Chem. Commun.*, 2010, **46**, 8043-8045.
14. M. Starck, J. D. Fradgley, S. Di Vita, J. A. Mosely, R. Pal and D. Parker, *Bioconjug. Chem.*, 2020, **31**, 229-240.
15. K. L. Gempf, S. J. Butler, A. M. Funk and D. Parker, *Chem. Commun.*, 2013, **49**, 9104-9106.
16. I. D. Herath, C. Breen, S. H. Hewitt, T. R. Berki, A. F. Kassir, C. Dodson, M. Judd, S. Jabar, N. Cox, G. Otting and S. J. Butler, *Chem. Eur. J.*, 2021, **27**, 13009-13023.
17. A. G. Cosby, J. J. Woods, P. Nawrocki, T. J. Sørensen, J. J. Wilson and E. Boros, *Chem. Sci.*, 2021, **12**, 9442-9451.
18. A. Shah, A. Roux, M. Starck, J. A. Mosely, M. Stevens, D. G. Norman, R. I. Hunter, H. El Mkami, G. M. Smith, D. Parker and J. E. Lovett, *Inorg. Chem.*, 2019, **58**, 3015-3025.